Microchimica Acta (2021) 188: 77
https://doi.org/10.1007/s00604-021-04737-w

ORIGINAL PAPER

2D metal azolate framework as nanozyme for amperometric detection of glucose at physiological pH and alkaline medium

Muhammad Adeel[1,2] · Vincenzo Canzonieri[2,3] · Salvatore Daniele[1] · Alberto Vomiero[1,4] · Flavio Rizzolio[1,2] · Md. Mahbubur Rahman[5]

Received: 26 October 2020 / Accepted: 29 January 2021 / Published online: 10 February 2021

Abstract

The synthesis of Co-based two-dimensional (2D) metal azolate framework nanosheets (MAF-5-Co^{II} NS) is described using a simple hydrothermal method. The product was isostructural to MAF-5 (Zn). The as-prepared MAF-5-Co^{II} NS exhibited high surface area (1155 m^2/g), purity, and crystallinity. The MAF-5-Co^{II} NS–modified screen-printed electrode (MAF-5-Co^{II} NS/SPE) was used for nonenzymatic detection of glucose in diluted human blood plasma (BP) samples with phosphate buffer saline (PBS, pH 7.4) and NaOH (0.1 M, pH 13.0) solutions. The MAF-5-Co^{II} NS nanozyme displayed good redox activity in both neutral and alkaline media with the formation of Co^{II}/Co^{III} redox pair, which induced the catalytic oxidation of glucose. Under the optimized detection potential, the sensor presented a chronoamperometric current response for the oxidation of glucose with two wide concentration ranges in PBS-diluted (62.80 to 180 μM and 305 to 8055 μM) and NaOH-diluted (58.90 to 117.6 μM and 180 to 10,055 μM) BP samples, which were within the limit of blood glucose levels of diabetic patients before (4.4–7.2 mM) and after (10 mM) meals (recommended by the American Diabetes Association). The sensor has a limit of detection of ca. 0.25 and 0.05 μM, respectively, and maximum sensitivity of ca. 36.55 and 1361.65 mA/cm^2/mM, respectively, in PBS- and NaOH-diluted BP samples. The sensor also displayed excellent stability in the neutral and alkaline media due to the existence of hydrophobic linkers (2-ethyl imidazole) in the MAF-5-Co^{II} NS, good repeatability and reproducibility, and interference-free signals. Thus, MAF-5-Co^{II} NS is a promising nanozyme for the development of the disposable type of sensor for glucose detection in human body fluids.

Keywords Metal azolate framework · Glucose detection · Chronoamperometry · Human blood plasma · Neutral and alkaline conditions

✉ Alberto Vomiero
alberto.vomiero@ltu.se

✉ Flavio Rizzolio
flavio.rizzolio@unive.it

✉ Md. Mahbubur Rahman
mahbub1982@kku.ac.kr

[1] Department of Molecular Sciences and Nanosystems, Ca'Foscari University of Venice, 30172 Venice-Mestre, Italy

[2] Pathology Unit, Centro di Riferimento Oncologico di Aviano (CRO) IRCCS, 33081 Aviano, Italy

[3] Department of Medical, Surgical and Health Sciences, University of Trieste, 34127 Trieste, Italy

[4] Division of Materials Science, Department of Engineering Sciences and Mathematics, Luleå University of Technology, SE-97187 Luleå, Sweden

[5] Department of Energy and Materials, Konkuk University, Chungju 27478, Republic of Korea

Introduction

Since the invention of the first-generation glucose sensor by Clark and Lyons in 1962, based on a glucose oxidase (GO_x) enzyme [1, 2], there have been many attempts on the evolution of glucose sensor technologies such as second and third generations. This is mainly due to the low-stability and complex immobilization processes of GO_x, even though it is highly selective for the catalytic oxidation of glucose [3]. GO_x can be irreversibly damaged at a temperature > 40 °C, loses catalytic activity at the pH below 2.0 or higher than 8.0, and is affected by the surfactants at a certain pH [4]. Furthermore, variable humidity and limited solubility of oxygen in body fluids can substantially influence the performance of GO_x-based glucose sensor. This is because variable humidity and oxygen deficit can modulate the concentration of oxygen and leads to the deviation of actual glucose concentration measured at the normal level of oxygen [4]. The

oxygen dependency of the first-generation glucose sensor is successfully eliminated in the second-generation glucose sensor by introducing a nonphysiological redox mediator that can transport electrons from the GO_x to the sensing electrode [5]. Then, a third-generation glucose sensor was developed based on the direct electron transfer between the GO_x and the sensing electrode, thus overcoming the necessity of both mediator and oxygen [6, 7]. These second- and third-generation glucose sensors, still based on GO_x, can successfully solve the oxygen dependency problems of the first-generation glucose sensors, widely used for self-monitoring of blood glucose levels; however, the stability issues of GO_x still apply. Moreover, these enzyme-based glucose sensors are hardly free from thermal or chemical deformation during their manufacturing processes, storage and usage [4].

Recently, the introduction of nanozymes or enzymeless catalysts has been attracting significant attention for the detection of glucose, which can successfully solve all the limitations of first- to third-generation glucose sensor technologies. In a nonenzymatic or so-called fourth-generation glucose sensor, nanostructured and catalytically active nanozymes are used as electrode modifiers that can catalyze the oxidation of glucose directly to gluconolactone, thus providing measurable electrical signals [4, 8]. The commonly used nanozymes for enzymeless detection of glucose are metal nanostructures (Ni, Pt, Au, Cu, and Co) [9, 10] and their alloys/composites [9–12], metal oxides and sulfides [3, 13, 14], graphene nanocomposite [15], and metal-organic frameworks (MOFs) [16–19]. Most of these nanozymes cannot catalyze the oxidation of glucose at physiological pH conditions, as they operate in basic medium, which limits the instant detection of glucose in biological fluids [8, 9]. The nonenzymatic detection of glucose in a basic medium directly through nanozyme-modified electrodes is also promising since it resolves the necessity of complex enzyme immobilization processes and demonstrates a new direction to detect glucose selectively without enzyme. However, the nonenzymatic sensing of glucose in a basic medium is time-consuming and requires costly pre-/post-conditioning of biological fluids before detection. This precludes the real-time monitoring of glucose directly from biological fluids. Therefore, there is an utmost need for novel materials that can directly oxidize glucose at physiological pH conditions and lead the nonenzymatic glucose sensor technology from bench to practical applications.

To date, a limited number of nanozymes have been reported for the enzymeless electrochemical oxidation of glucose at physiological pH conditions, which has recently been summarized by our research group [20]. So far, bare Pt and Au nanostructures and their composites are the widely investigated nanozymes for the electrochemical oxidation of glucose at physiological pH, including Au/Pt black/Nafion [21], Pt electrodes [22], carbon-supported Pt_xFe alloy nanoparticles (NPs) [23], PtNi NP/graphene composites [24], TiO_2/poly(3-aminophenyl boronic acid)/Au NP composites [25], PtNi NPs [11], and Au NP/carbon nanotubes [26]. Though the Pt and Au noble metal nanostructures and their alloys/composites presented good catalytic activity for enzymeless oxidation of glucose at physiological pH, both of them displayed the disadvantages of high-cost and suffered from the poisoning effect from adsorbed intermediates [26]. In addition, Pt-based materials displayed a strong ability of protein adsorption and poor selectivity toward glucose oxidation, due to the capability of oxidizing other biomolecules [4]. This can prompt an unstable signal, and, as a result, the sensor is unable to respond correctly to variations of glucose concentration. Furthermore, the large-scale synthesis of these expensive Pt and Au composites nanozymes is tedious and time-consuming, which restricts their commercial application for glucose sensing with high reproducibility. Thus, there is a necessity in developing novel nanozymes that can catalyze the oxidation of glucose with high selectivity, sensitivity, and specificity at physiological pH as a single material.

Recently, metal-organic frameworks (MOFs), porous coordination polymers of metal ions and organic linkers, have attracted massive interest in the nonenzymatic detection of glucose due to their organic (as linkers) and inorganic (central metal atoms) properties [16, 17]. This is owing to the combination of metal ions or their clusters into the MOFs, which displayed good electrochemical redox activity to catalyze the oxidation of glucose [27]. Additionally, MOFs exhibit various shapes and structures (including one-, two-, and three-dimensional assembly) and high surface-to-volume ratio, which provides an improved electrocatalytic activity for the oxidation reaction of glucose [16, 17] and other targeted biomolecules, including H_2O_2 [28], L-cysteine [29], tryptophan [30] and glutathione [31]. Nevertheless, most of the reported MOFs and MOF composites cannot catalyze the oxidation of glucose at physiological pH media. They typically work at basic pH [16, 17, 32]. Additionally, the low chemical and electrochemical stability of MOFs in an aqueous (neutral, acidic, and basic) medium and the low electrical conductivity restrict their practical application for nonenzymatic glucose sensing [28]. To overcome some of these limitations of MOFs, metal azolate frameworks (MAFs), a subclass of MOF materials, have been proposed as an attractive alternative to MOFs, for the devolvement of nonenzymatic glucose sensors with high stability and reproducibility [17]. In fact, MAFs exhibit high stability in aqueous media, due to the presence of inert/hydrophobic linkers (e.g., imidazolate, 1,2,4-triazolate, and pyrazolate) adjacent to the metal centers [33, 34]. Despite this characteristic, the application of MAFs for nonenzymatic glucose detection is hardly found in the literature. This is possibly due to the fact that common MAFs still exhibit poor electrical conductivity and reduced redox activity in both physiological pH and basic media. Recently, Lopa et al. [17] have developed a MAF, which can catalyze glucose oxidation in an alkaline medium and within a narrow dynamic range,

which is not appropriate to detect glucose within the relevant glucose concentration range in biological samples. Hence, there appears the need to develop a novel MAF, exhibiting high electrochemical stability and ability to catalyze the oxidation of glucose in both physiological pH and alkaline media with high sensitivity and selectivity.

Herein, a two-dimensional (2D) nanosheet of MAF-5-Co^{II} (MAF-5-Co^{II} NS) was synthesized via a simple hydrothermal method. MAF-5-Co^{II} was selected due to its scalable and easy synthesis at room temperature without the necessity for high vacuum and high-temperature conditions, allowing the applicability of this material at a large scale. Besides, Co metal is less expensive compared to Au and Pt, and it is highly electrocatalytic and electrochemically stable for the oxidation of glucose at neutral conditions. The 2D morphologies of MAF-5-Co^{II} NS, with thicknesses at nanoscale levels, can provide the desired high surface-to-volume ratio and, consequently, a large number of electrocatalytic active sites, able to display good catalytic activity for the oxidation of glucose in both physiological pH and alkaline medium. In this paper, in particular, a MAF-5-Co^{II} NS nanozyme–modified screen-printed electrode (MAF-5-Co^{II} NS/SPE) sensor is fabricated and then used for enzymeless detection of glucose in blood plasma (BP) samples diluted with phosphate buffer saline (PBS, pH 7.4) and NaOH (0.1 M) solutions. The sensor presents high sensitivity, specificity, electrochemical stability, and good accuracy in both (PBS, pH 7.4) and NaOH (0.1 M) media.

Experimental section

Materials and reagents

Cobalt (II) acetate ($Co(OAc)_2$) (99.995% trace metals basis), 2-ethylimidazole (98%) (EIM), benzene (99.9%), cyclohexane (99.5%), ethanol (99.99%), D-(+)- glucose (99.5%), fructose, lactose, galactose, Nafion® 117 (5% in a mixture of low aliphatic alcohols and water), and NaOH were purchased from Sigma-Aldrich. Dulbecco's PBS (pH 7.4) without calcium and magnesium chloride was procured from Thermo Fisher Scientific. SPE-110 was purchased from Ω Metrohm DropSens. Ultrapure water was obtained from Milli Q Biocell water purifying system and used throughout the experiment. PBS with a pH of 7.4 and aqueous NaOH (0.1 M, pH 13.0) were used throughout the experiment unless otherwise stated.

Apparatus and measurements

The morphology of the MAF was examined by a field-emission scanning electron microscope (FE-SEM, Carl Zeiss Sigma VP) and a high-resolution transmission electron (HR-TEM, JEM-2100 (HRP)). Elemental analyses were executed using energy-dispersive X-ray spectroscopy (EDS) (Quantax 200) equipped with the FE-SEM. The crystallographic phase of the sample was collected by an X-ray diffractometer (Philips Xpert, Cu K_α radiation). The elemental composition and the oxidation state of the sample were examined with an X-ray photoelectron spectroscopy system (XPS, Thermo Scientific™ K-Alpha, Thermo Fisher Scientific). The functional groups in the MAF were characterized by Fourier transform infrared (FTIR) spectroscopy (MIDAC, M4000). Thermogravimetric analysis (TGA) was performed in the temperature range 30–700 °C in atmospheric conditions. The N_2 adsorption isotherm was obtained at −190 °C, after evacuation at 110 °C for 12 h, using a surface area analyzer (Micromeritics, Tristar II 3020, USA). All electrochemical measurements were performed using a CHI760B potentiostat (CH Instrument, Texas, USA). Disposable screen-printed electrodes (SPEs) (from DropSens Metrohm), in the three-electrode configuration, consisted of a carbon disk working electrode (active area 0.125 cm^2), a carbon ring as an auxiliary electrode, and an Ag/AgCl as the reference electrode. The working electrode was coated with MAF-5-Co^{II} NS (MAF-5-Co^{II} NS/SPE) as specified below. For comparison, measurements were also performed using the MAF-5-Co^{II} NS-free naked carbon disk of SPE.

Synthesis of MAF-5-Co^{II} NS

Figure 1a shows the schematic of the synthesis of MAF-5-Co^{II} NS. Briefly, 0.1 g of $Co(OAc)_2$ was dissolved in water (25 mL) as a first solution. A second solution was prepared by dissolving 0.3 g of EIM in a mixture of water and benzene (65:10 *v*/v). These solutions were rapidly mixed and stirred at room temperature for 30 min. Then, the resultant blue-colored suspension was centrifuged at 6000 RPM for 10 min. The precipitate was washed with water and ethanol several times by the centrifuge method. Finally, the blue-colored powder was dried in a vacuum drying oven at 100 °C for 2 h and stored for further characterizations and applications.

Preparation of glucose sensor

A suspension of MAF-5-Co^{II} NS (2 mg/mL) was dispersed in a medium containing ethanol and Nafion®117 (1.5:0.5 *v*/v) by bath sonication for 1 h. Note that Nafion®117 is acting as a binder for the attachment of MAF-5-Co^{II} NS onto the SPE electrode. Around 20 μL of the above suspension was drop cast onto the carbon disk working electrode of SPE and dried at 60 °C for 1 h. The as-prepared MAF-5-Co^{II} NS/SPE was directly used for the detection of glucose.

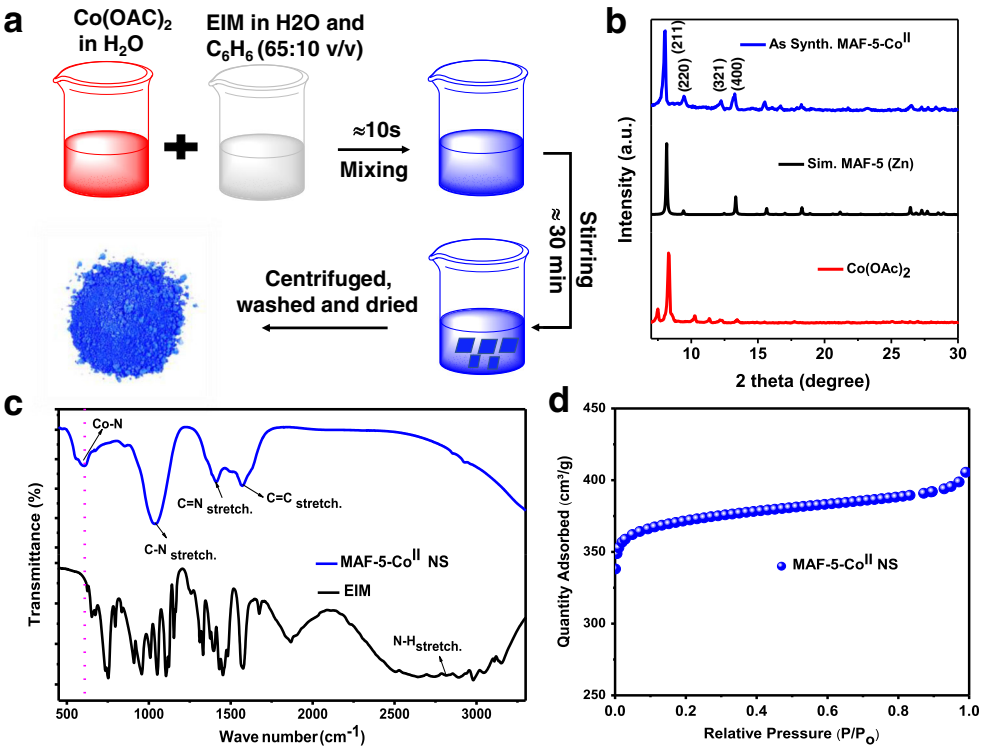

Fig. 1 **a** schematic of the synthesis of MAF-5-Co^{II} NS. **b** XRD patterns of MAF-5-Co^{II} NS and $Co(OAc)_2$ precursor together with simulated XRD pattern of MAF-5 (Zn). **c** FTIR spectra of MAF-5-Co^{II} NS and EIM. **d** N_2 adsorption isotherm of MAF-5-Co^{II} NS

Results and discussions

XRD, FTIR, and surface area analyses of MAF-5-Co^{II} NS

Figure 1b shows the X-ray diffraction (XRD) pattern of the synthesized MAF-5-Co^{II} NS, of $Co(OAc)_2$ precursor, and that simulated for MAF-5 (Zn). To elucidate the exact simulated and fingerprinted XRD pattern of the MAF-5-Co^{II}, the preparation of single-crystal analysis and the corresponding XRD analysis was beyond the scope of this research. It is noteworthy that there is no available computed or single-crystal analysis of crystallographic information for MAF-5-Co^{II}. However, the XRD pattern of MAF-5-Co^{II} NS and MAF-5 (Zn) matches well, indicating that MAF-5-Co^{II} NS is isostructural with MAF-5 (Zn) [33, 35]. The sharp and intense major XRD peaks of MAF-5-Co^{II} with the *hkl* reflections of (211), (220), (321), (400), (332), and (521) at 2θ angle values of ca. 8.05, 9.51, 12.25, 13.25, 15.51 and 18.25°, respectively, point to its high crystallinity. The major XRD peaks of $Co(OAc)_2$ precursor was located at 2θ angle values of 7.46, 8.35 and 10.30°, which do not overlap with the XRD peaks of MAF-5-Co^{II}, suggesting the successful synthesis of MAF-5-Co^{II} and its high purity. FTIR spectra of MAF-5-Co^{II} NS and EIM were measured to investigate the nature of the chemical bonding and are shown in Fig. 1c. The FTIR spectrum of EIM shows the characteristic strong absorption bands of C–N, C=N, and C=C stretching at ca. 1046, 1457, and 1570 cm^{-1}, respectively, together with a wide band of N–H stretching in the range of ca. 2500–3150 cm^{-1} [17]. The synthesized MAF-5-Co^{II} NS shows a similar strong absorption band of C–N, C=N, and C=C at ca. 1050, 1450, and 1570 cm^{-1}, respectively. However, the FTIR spectra of MAF-5-Co^{II} NS exhibits a strong decrease of the N–H stretching band and the appearance of a strong band at 610 cm^{-1}. The latter can be assigned to the Co–N stretching, due to the formation of a Co–N coordination bond [17], which is in agreement with the bonds expected in MAF-5-Co^{II} NS.

The surface area (SA_{BET}) of the MAF-5-Co^{II} NS was measured from the N_2 adsorption isotherm (Fig. 1d). SA_{BET} of ca. 1155 m^2/g was found. The high SA_{BET} MAF-5-Co^{II} NS is advantageous, as it allows increasing the number of catalytically active sites, and this can provide an increased rate of reaction.

We also investigated the thermal stability of the MAF-5-Co^{II} NS using TGA (Fig. S1). The TGA plot displayed two-steps weight loss. The first-step weight loss of ca. 10% up to 200 °C can be ascribed to the removal of chemisorbed water, guest molecules, and unreacted species [16, 17]. The sharper second-step weight loss of ca. 35% can be ascribed to the decomposition of the MAF-5-Co^{II} framework. This implies that MAF-5-Co^{II} is highly stable and well suitable for the development of sensors functioning at room temperature.

Morphological characterization of MAF-5-Co^{II} NS

The morphologies of the MAF-5-Co^{II} NS was examined by FE-SEM and HR-TEM. The FE-SEM image of MAF-5-Co^{II} NS (Fig. 2a) indicated the formation of 2D NS. The HR-TEM

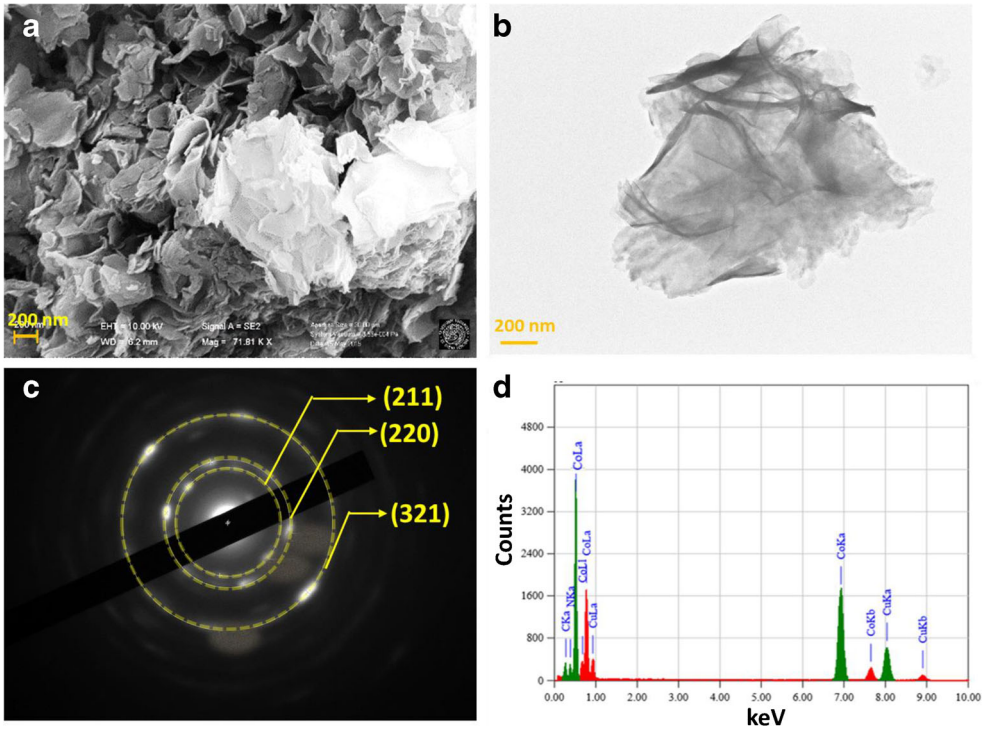

Fig. 2 **a** FE-SEM and **b** HR-TEM images of MAF-5-Co^{II} NS. **b** SAED pattern and **d** EDS spectra of MAF-5-Co^{II} NS

image (Fig. 2b) further designates the formation of 2D MAF-5-Co^{II} NS. The high transparency of the electron beam of the MAF in the HR-TEM image suggests the formation of thinner NS without the existence of aggregation. The SAED pattern of the MAF-5-Co^{II} NS exhibited a bright ring pattern with bright spots with the *hkl* reflections of (211), (220), and (321) (Fig. 2c). This is consistent with the XRD results and further indicates the good crystallinity of MAF-5-Co^{II} NS. The EDS analysis of MAF-5-Co^{II} NS (Fig. 2d) shows peaks coming from Co, N, and C atoms (the Cu peaks originating from the HR-TEM grid), further indicating the formation of MAF-5-Co^{II} NS with high purity.

XPS characterization of MAF-5-Co^{II} NS

The elemental composition and the oxidation state of Co in MAF were investigated by XPS. Figure 3a shows a survey XPS spectrum (100–900 eV) of MAF-5-Co^{II} NS, in which the characteristic peaks of Co, N, and C elements appear. The additional peak characteristic of elemental O arises, conceivably, from chemisorbed O_2. Figures 3b–d show the core-level XPS spectra of C 1s, N 1s, and Co 2p, respectively. The de-convoluted high-resolution spectrum of C 1s exhibits three peaks with variable intensity at the binding energies (BE) of 283.40, 284.80, and 287.50 eV. This could be ascribed to the existence of C–C/C=C, C–N, and C=N bonding characteristics, respectively, in the MAF-5-Co^{II} NS and agree well with literature reports [36, 37]. The de-convoluted core-level N 1s spectrum shows two peaks of C=N and C–N at the BEs of 397.60 and 398.70 eV, respectively [36]. The bonding nature of C–C and C–N in the C 1s and N 1s spectra indicates the presence of EIM linkers in the MAF-5-Co^{II} NS. The high-resolution XPS spectra of Co 2p exhibit two main peaks at the BEs of ca. 779.80 and 795.60 eV with the separation of 15.8 eV, which is consistent with the previous reports [17, 38]. The former peak could be assigned to the Co $2p_{3/2}$, while the latter to the Co $2p_{1/2}$. Both Co $2p_{3/2}$ and Co $2p_{1/2}$ peaks showed their corresponding strong satellite peaks at the BEs of ca. 784.22 and 801.30 eV, respectively. This result suggests that the oxidation state of Co in the MAF is +2 [18, 39].

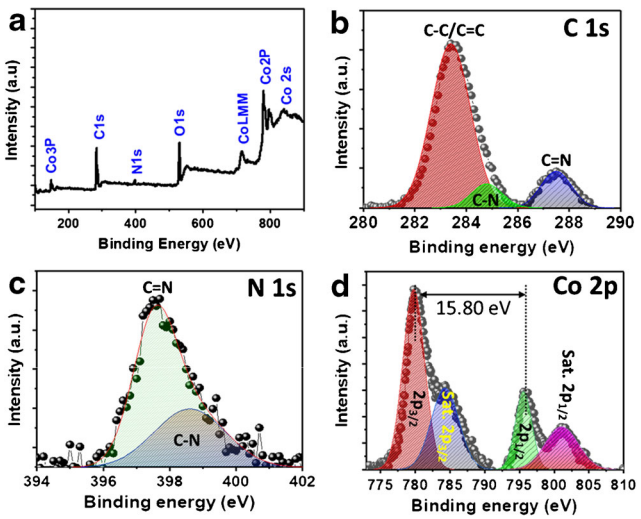

Fig. 3 **a** XPS survey spectra of MAF-5-Co^{II} NS. High-resolution XPS spectra of **b** C 1s, **c** N 1s, and **d** Co 2p in MAF-5-Co^{II} NS

Electrochemical characterization MAF-5-Co^{II} NS for glucose oxidation

Figure 4a shows the schematic representation of the preparation of the MAF-5-Co^{II} NS–modified SPE electrode (MAF-5-Co^{II} NS/SPE), while the detailed procedure is described in Section 2.4. Preliminarily, the MAF-5-Co^{II} NS/SPE electrode was characterized by cyclic voltammetry (CV) in a solution containing 5 mM $[Fe(CN)_6]^{3-/4-}$ redox couple and 1 M KCl (Fig. S2). At the bare SPE, the CV was characterized by a couple of drown-out and distorted waves having a quite large peak-to-peak separation, due, conceivably, to a high ohmic drop. The CV recorded at the MAF-5-Co^{II} NS/SPE displayed a high charging current, congruently with the high real surface area and mesoporous nature of the MAF material [40]. The current densities of both oxidation and reduction peaks were lower, while the peak-to-peak separation decreased to about 60 mV. Seemingly, both anodic and cathodic peaks shifted toward less positive potentials, which would suggest a catalytic effect due to the material deposited onto the SPE surface. The observed changes in the CV features can be, conceivably, ascribed to the general low conductivity of MOF materials [17, 28] and to the fact that the fairly reversible, one-electron process of the $[Fe(CN)_6]^{3-/4-}$ system probably occurred at the relatively small fraction of the SPE surface free from the MAF-5-Co^{II} NS material. This could provide a better-defined anodic/cathodic voltammetric pattern. The electroactive surface area ($A_{eff.}$) of the bare SPE and MAF-5-Co^{II} NS/SPE were ca. 4.3×10^{-2} and 2.9×10^{-2} cm^2, respectively (see supporting information for details), which is consistent with the electrocatalytic activity of MAF-5-Co^{II} NS/SPE electrode for $[Fe(CN)_6]^{3-/4-}$ redox couple.

Figure 4b shows CVs recorded at uncoated SPE and MAF-5-Co^{II} NS/SPE in PBS in the absence and presence of 2 mM of glucose. As is evident, at the bare SPE, in both cases, negligible currents are recorded. This is consistent with results reported previously for carbon-based electrodes, where, essentially, no process due to glucose oxidation was recorded, over the potential zone examined here [41]. At the MAF-5-Co^{II} NS/SPE, in the absence of glucose, small anodic/cathodic features at potentials anodic to 0.3 V are observed, conceivably due to the Co^{2+}/Co^{3+} redox couple of the nanostructured material. Instead, in the presence of glucose, an oxidation process, starting at about 0.3 V, develops, while an associated reduction process appears on scan reversal. Both the anodic (after 0.3 V) and cathodic current densities have increased substantially, though no oxidation peak is detectable. The current increase can be ascribed to the catalytic action of MAF-5-Co^{II} NS towards glucose oxidation. Using the MAF-5-Co^{II} NS/SPE, a series of measurements was also performed at different scan rates (Fig. 4c). Both anodic and cathodic current density for glucose oxidation increased as the scan rate increased. The anodic current density (J) at 0.4 V was found to be proportional to the square root of the scan rate (inset of Fig. 4c). The linear regression analysis of experimental data provided the equation: $J\ (\mu A/cm^2) = 1.57\ (\pm 0.02) \times \nu^{1/2}\ (mV/s)^{1/2} - 2.14\ (\pm\ 0.21;\ R^2 = 0.997)$, suggesting the occurrence of a diffusion-controlled oxidation process [42].

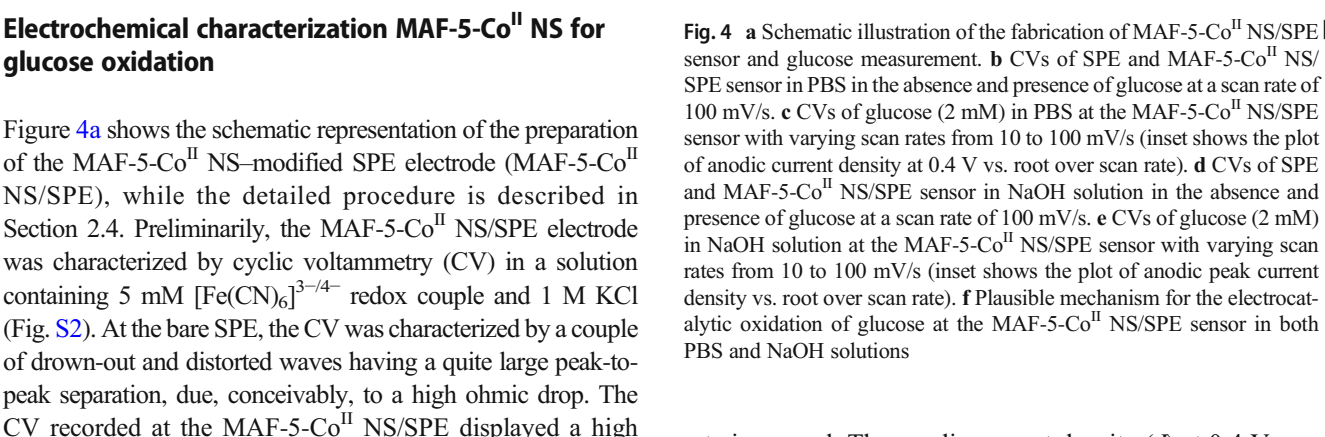

Fig. 4 **a** Schematic illustration of the fabrication of MAF-5-Co^{II} NS/SPE sensor and glucose measurement. **b** CVs of SPE and MAF-5-Co^{II} NS/SPE sensor in PBS in the absence and presence of glucose at a scan rate of 100 mV/s. **c** CVs of glucose (2 mM) in PBS at the MAF-5-Co^{II} NS/SPE sensor with varying scan rates from 10 to 100 mV/s (inset shows the plot of anodic current density at 0.4 V vs. root over scan rate). **d** CVs of SPE and MAF-5-Co^{II} NS/SPE sensor in NaOH solution in the absence and presence of glucose at a scan rate of 100 mV/s. **e** CVs of glucose (2 mM) in NaOH solution at the MAF-5-Co^{II} NS/SPE sensor with varying scan rates from 10 to 100 mV/s (inset shows the plot of anodic peak current density vs. root over scan rate). **f** Plausible mechanism for the electrocatalytic oxidation of glucose at the MAF-5-Co^{II} NS/SPE sensor in both PBS and NaOH solutions

An investigation similar to that described above in PBS was also performed in 0.1 M NaOH solution. Figure 4d shows CVs obtained at SPE and MAF-5-Co^{II} NS/SPE in the absence and presence of 2 mM of glucose. Again, the bare SPE did not exhibit any redox process both in the absence and presence of glucose. MAF-5-Co^{II} NS/SPE displayed clearly a couple of oxidation (I) and reduction (I') peaks at ca. 0.35 and 0.17 V, respectively, which can be attributed to the Co^{II}/Co^{III} redox system of the MAF nanostructured material. A similar explanation was given for the MOF family MAF-4-Co^{II}, MIL-53-Cr^{III}, and CPO-27-Ni^{II}, involving the redox couple of the metal ions present in their structures [16, 17, 28]. The addition of 2 mM glucose to the 0.1 M NaOH solution provided an increase of the oxidation current density and a shift of the peak potential toward less positive values. These results are a clear indication of the high electrocatalytic activity of MAF-5-Co^{II} NS toward the oxidation of glucose to gluconolactone [16, 17]. CVs performed at different scan rates, over the range 10–100 mV/s, also demonstrated that the oxidation peak current density of glucose varied linearly with the square root of the scan rate (Fig. 4e and inset of Fig. 4e). The linear regression analysis of the experimental data provided the equation: $J\ (\mu A/cm^2) = 102.60\ (\pm\ 1.61) \times \nu^{1/2}\ (mV/s)^{1/2} - 203.10\ (\pm\ 11.97)$ ($R^2 = 0.998$), suggesting the occurrence of a diffusion-controlled oxidation process of glucose [42].

Based on the above results and by analogy with previously reported works for similar materials [17], the enzymeless electrochemical oxidation of glucose at the MAF-5-Co^{II} NS/SPE, in both PBS and NaOH solutions, can be summarized as follows:

$$MAF{-}5{-}Co^{II} \rightarrow MAF{-}5{-}Co^{III} + e^{-} \quad (1)$$

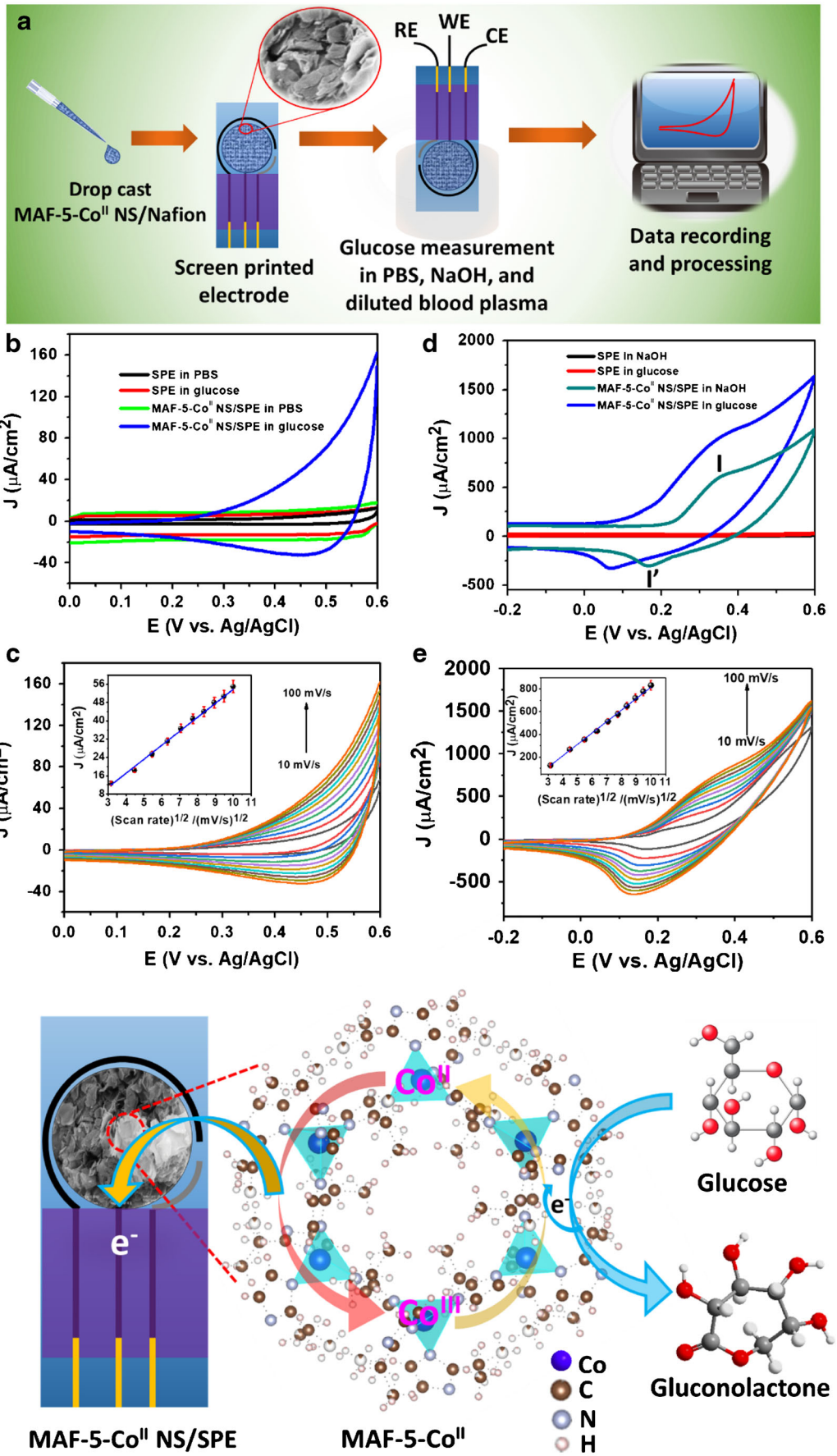
a
RE
WE
CE
Drop cast
MAF-5-Co^{II} NS/Nafion
Screen printed electrode
Glucose measurement in PBS, NaOH, and diluted blood plasma
Data recording and processing
b
SPE in PBS
SPE in glucose
MAF-5-Co^{II} NS/SPE in PBS
MAF-5-Co^{II} NS/SPE in glucose
J (μA/cm^2)
E (V vs. Ag/AgCl)
d
SPE in NaOH
SPE in glucose
MAF-5-Co^{II} NS/SPE in NaOH
MAF-5-Co^{II} NS/SPE in glucose
I
I'
J (μA/cm^2)
E (V vs. Ag/AgCl)
c
100 mV/s
10 mV/s
J (μA/cm^2)
(Scan rate)$^{1/2}$ /(mV/s)$^{1/2}$
E (V vs. Ag/AgCl)
e
100 mV/s
10 mV/s
J (μA/cm^2)
(Scan rate)$^{1/2}$ /(mV/s)$^{1/2}$
E (V vs. Ag/AgCl)
e$^-$
Co^{II}
Co^{III}
Glucose
Gluconolactone
Co
C
N
H
MAF-5-Co^{II} NS/SPE
MAF-5-Co^{II}

$$MAF{-}5{-}Co^{III} + glucose \rightarrow MAF{-}5{-}Co^{II} + gluconolactone + H^{+} \quad (2)$$

A schematic representation of the mechanism is also provided in Fig. 4f. Therefore, the porous structure and the high surface area of the of MAF-5-Co^{II} NS favor the interaction between the active form of MAF (i.e., the Co(III) site) with glucose. It must be noted that both redox activity of the MAF-5-Co^{II} NS material and its catalytic activity toward the glucose oxidation are lower in neutral pH compared to those in the alkaline medium.

Detection of glucose in PBS and NaOH

Chronoamperometry (CA) was used to investigate the effect of concentration of glucose on current density. Since with this technique the applied potential plays an important role on the sensitivity of the method [16], preliminarily, the most suited potential was optimized both in PBS and 0.1 M NaOH solutions containing 2 mM of glucose. The potential ranges explored were from 0.35 to 0.55 V in PBS and from 0.3 to 0.45 V in 0.1 M NaOH. Figure S3 shows typical current against time profiles obtained under the various conditions, while the steady-state currents at the various potentials are summarized in the insets in Figs. 5a and b. It is evident that the steady-state current increases, as the potential is made more positive. However, it must be considered that higher applied potentials could affect the selectivity of the sensor, due to the presence of other oxidizing compounds. To minimize interference effects, we selected 0.45 and 0.35 V as the constant potentials to be applied for the detection of glucose in PBS and NaOH solutions, respectively.

Figures 5a and b (main pictures) show the CA plots at a range of glucose concentrations in PBS and NaOH solutions, respectively. The plots of steady-state oxidation current against glucose concentration are included in the insets (right side) of Fig. 5a and b. As is evident, in both media, current responses increase by increasing the glucose concentration. However, linearity is observed in two well-defined concentration ranges. Dynamic ranges, linear regression equations, sensitivities, and LODs under the different conditions are summarized in Table 1. LODs were obtained at a signal-to-noise ratio (S/N) of 3. The occurrence of the two linear ranges, observed above in the calibration plots, has been reported previously for other MOFs/MAFs [23, 24]. For the glucose oxidation process, it was explained as due to the accumulation of gluconolactone oxidation product within the porous structure of the material. At low concentrations, glucose spreads within the sensor structure and is quickly oxidized by the availability of a large number of active sites, providing current responses characterized by high slope in the calibration plot. On the other hand, at higher glucose concentrations, the higher amount of adsorbed oxidation product can act as a barrier for glucose diffusion, which leads to current responses with a lower slope in the calibration plot [43].

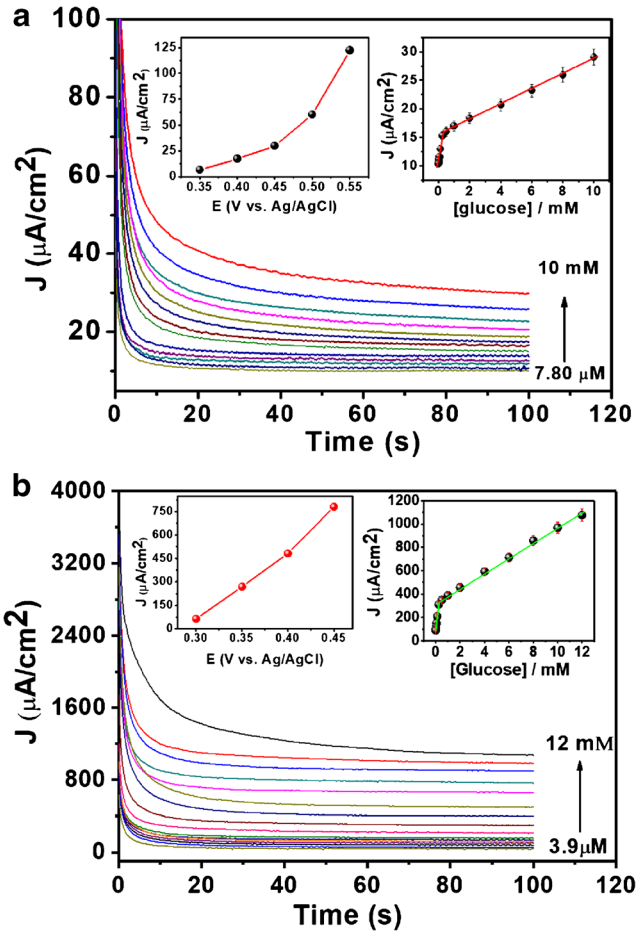

Fig. 5 **a** CA responses of glucose oxidation in PBS with varying concentrations from 7.80 to 10 mM (7.81, 15.6, 31.25, 62.6, 125, 250, 500, 1000, 2000, 4000, 6000, 8000, and 10,000 μM, respectively) at the MAF-5-Co^{II} NS/SPE sensor at an applied potential of 0.45 V (inset shows the plots of current density vs. applied potential for the oxidation of glucose (2 mM) and current density vs. [glucose] obtained from the CA responses). **b** CA responses of glucose oxidation in NaOH solution with varying concentrations from 7.80 to 10 mM (3.9, 15.6, 31.25, 62.6, 125, 250, 500, 1000, 2000, 4000, 6000, 8000, 10,000, and 12,000 μM, respectively) at the MAF-5-Co^{II} NS/SPE sensor at an applied potential of 0.35 V (inset shows the plots of current density vs. applied potential for the oxidation of glucose (2 mM) and current density vs. [glucose] obtained from the CA responses)

Considering data shown in Table 1, it is evident that the analytical performance (e.g., sensitivity, LOD) of the sensor is better in NaOH solution than in PBS. This could be ascribed to the improved efficiency of MAF-5-Co^{II}/MAF-5-Co^{III} redox pair in recycling its active form. In general, the analytical performance of the investigated sensor in PBS is comparable to others involving nanomaterial systems used for the nonenzymatic glucose oxidation, while it is much higher in alkaline media as summarized in Tables S1 and S2, respectively. Therefore, MAF-5-Co^{II} NS represents a promising low-cost

Table 1 Analytical performance of the MAF-5-Co^{II} NS/SPE sensor under various experimental conditions. C_{Glu} is the concentration of glucose

Medium	Dynamic range	Linear regression equation (R^2)	Sensitivity μA/cm^2/mM	LOD μM
PBS	0.5 μM–10,000 mM	J (μA/cm^2)=1.32 (± 0.03)×C_{Glu} (mM)+ 15.50 (±0.13) (R^2=0.997)	1.32	–
	7.81 μM–250 μM	J (μA/cm^2)=24.22 (±1.50)×C_{Glu} (mM)+ 10.60 (±0.14) (R^2=0.985)	24.22	0.30
PBS-diluted BP	305 μM−8055 μM	J (μA/cm^2)=2.50 (±0.14)×C_{Glu} (mM)+ 7.30 (±0.72) (R^2=0.988)	2.50	–
	62.80–180 μM	J (μA/cm^2)=36.55 (±1.55)×C_{Glu} (mM)+ 1.98 (±0.17) (R^2=0.997)	36.55	0.25
NaOH	250 μM–12 mM	J (μA/cm^2)=66.50 (±1.76)×C_{Glu} (mM)+ 313.0 (±6.20) (R^2=0.995)	66.50	
	3.90–125 μM	J (μA/cm^2)=1012.70 (±25.90)×C_{Glu} (mM)+86.20 (±1.10) (R^2=0.997)	1012.70	0.09
NaOH-diluted BP	180 μM−10,055 mM	J (μA/cm^2)=80.43 (±0.35)×C_{Glu} (mM)+ 114.70 (±1.75) (R^2=0.999)	80.43	
	58.90–117.6 μM	J (μA/cm^2)=1361.65 (±78.51)×C_{Glu} (mM)+42.43 (±6.44) (R^2=0.999)	1361.65	0.05

material for the detection of glucose from biological fluids in physiological pH and alkaline media.

Detection of glucose in diluted blood plasma

Blood plasma (BP) samples were collected from 40 healthy volunteer donors without having diabetes at Centro di Riferimento Oncologico di Aviano, National Cancer Hospital, Italy. The average normal concentration of glucose in the BP is considered equal to 5.5 mM [44]. A series of PBS or 0.1 M NaOH solution–diluted BP samples (100 times) were spiked with glucose in the range from 3.9 to 10 mM. In these solutions, the total concentrations of glucose are the sum of spiked concentrations and the normal concentration after dilution (55 μM). The corresponding CA plots for glucose oxidation at the MAF-5-Co^{II} NS/SPE sensor are shown in Figs. 6a and b, in PBS- and NaOH-diluted BP, respectively. For both cases, the steady-state current of glucose oxidation increased with increasing the concentration of glucose, which also exhibited linear responses in two concentration ranges (insets of Fig. 6a and b), as observed above in synthetic PBS and NaOH solutions (Fig. 5). Dynamic ranges, linear regression equations, sensitivities, and LODs in both PBS and 0.1 M NaOH–diluted BP samples are included in Table 1. These results indicate that the MAF-5-Co^{II} NS is suitable for the development of disposable type sensors for point-of-care detection of glucose concentration in biological fluids at physiological pH and alkaline medium.

Stability, selectivity, interference studies, repeatability, and reproducibility

Long-term stability of the electrode materials is essential to develop a reliable glucose sensor. This aspect was investigated by CA (Fig. 6c), using diluted BP samples (with either PBS or 0.1 M NaOH), spiked with 2 mM of glucose. It was found that after 1000s, the glucose oxidation currents decreased of 3.95 and 8.10%, in PBS- and NaOH-diluted BP samples, respectively, denoting good stability for a series of point-of-care measurements. Furthermore, the stability of the sensor was also assessed by performing a series of consecutive CVs cycles, using diluted BP samples (with either PBS or 0.1 M NaOH), spiked with 2 mM of glucose, as shown in Fig. 6d and e, respectively. After 100 CV cycles, the anodic current for the oxidation of glucose in both PBS- and NaOH-diluted BP samples remained essentially unchanged, suggesting the stability of the material over a larger potential range.

The electrochemical stability of the MAF-5-Co^{II} NS was further evaluated by measuring the core-level XPS spectra of Co 2p (Fig. S4) after performing 100 CV cycles in both PBS- and NaOH-diluted BP samples. Both the XPS spectra showed the unaltered peak position with similar intensities, which is well-matched with the Co 2p spectra of as-synthesized MAF-5-Co^{II} NS (Fig. 3d), suggesting the high stability of MAF-5-Co^{II} in both alkaline and neutral media. This can be ascribed to the existence of inert/hydrophobic EIM linkers in the MAF-5-Co^{II}, which can easily hinder the attack of solvent (water) or other molecules to the coordinated metal centers.

The selectivity of the sensor was investigated by CV using other common sugar molecules, namely, fructose, galactose, and lactose. Figure S5 shows the CVs for the oxidation of fructose, galactose, and lactose (2 mM each) in PBS. The almost unaltered CV responses for the oxidation of these sugar molecules compared to the CV of the MAF-5-Co^{II} NS/SPE suggest the good specificity of the sensor for the oxidation of glucose. The interference effect of the sensor for the oxidation of glucose was investigated by CA in both PBS- and NaOH-diluted BP samples, spiked with 2 mM glucose and 5 mM

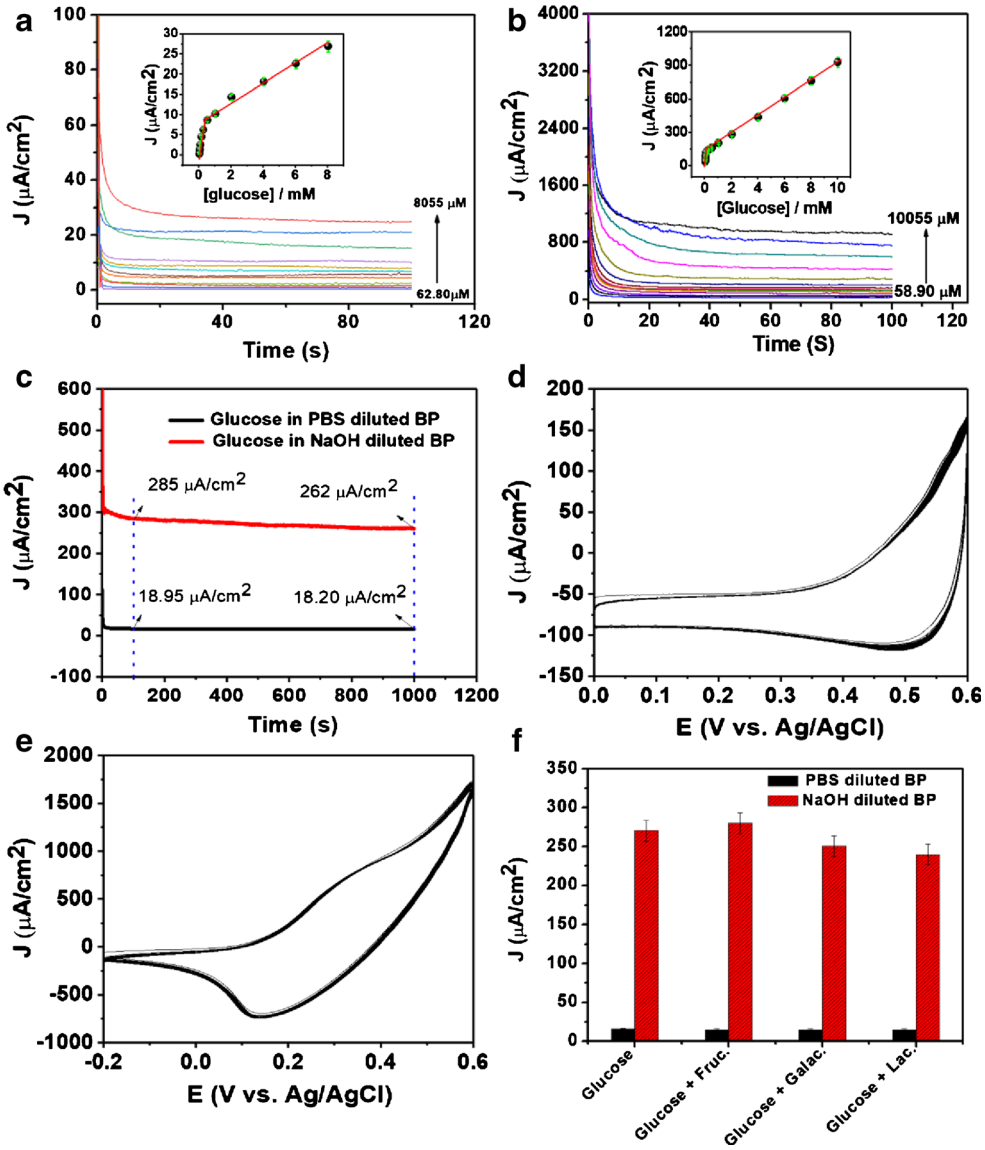

Fig. 6 **a** CA responses of glucose oxidation in PBS-diluted BP samples with varying concentrations (62.80, 70.60, 86.25, 117.60, 180, 305, 555, 1055, 2055, 4055, 6055, and 8055 μM, respectively) at the MAF-5-Co^{II} NS/SPE sensor at an applied potential of 0.45 V (inset shows the plot of current density vs. [glucose]). **b** CA responses of glucose oxidation in NaOH-diluted BP samples solution with varying concentrations (58.90, 70.60, 86.25, 117.6, 180, 305, 555, 1055, 2055, 4055, 6055, 8055, and 10,055 μM, respectively) at the MAF-5-Co^{II} NS/SPE sensor at an applied potential of 0.35 V (inset shows the plot of current density vs. [glucose]). **c** CA responses of PBS and NaOH solution–diluted BP samples with the spiked glucose concentration of 2 mM for 1000s. Consecutive CV sweeping (100 cycles) of the MAF-5-Co^{II} NS/SPE sensor in glucose (2 mM) spiked **d** PBS- and **e** NaOH-diluted BP samples at a scan rate of 100 mV/s. **f** Bar diagram of the glucose (2 mM) oxidation current responses in the absence and presence of different interferences

each of fructose, galactose, and lactose. Figure 6f summarizes the steady-state oxidation current thus obtained, while the corresponding CA signals are shown in Fig. S6. The variation of the glucose oxidation current in the presence of interfering species was 5.6, 6.4, and 5.2%, in PBS-diluted BP samples and 3.51, 7.4, and 12.2%, in NaOH-diluted BP samples, for fructose, galactose, and lactose, respectively. These results validate the good selectivity of the sensor for nonenzymatic detection of glucose in BP.

The reproducibility of the sensor preparation was tested using five independent sensors. The corresponding CA responses are shown in Fig. S7; the relative standard deviation (RSD) in the oxidation current of 2 mM glucose was ca. 1.40 and 8.20%, for PBS- and NaOH-diluted glucose spiked BP samples, respectively.

The repeatability of the sensor was studied after storing the sensor for 3weeks in normal atmospheric conditions. The CA responses for 2 mM glucose oxidation in PBS- and NaOH-diluted BP samples, measured every week interval, are shown in Fig. S8. RSD of 2.35 and 4.20% for PBS- and NaOH-diluted BP samples, respectively, was found, indicating the suitability of MAF-5-Co^{II} NS for the development of a disposable glucose measurement system with high reproducibility and repeatability.

Conclusions

We successfully prepared a 2D MAF-5-Co^{II} NS nanozyme–modified SPE electrode for the detection of glucose in PBS- and NaOH-diluted BP samples. The MAF-5-Co^{II} NS was synthesized by a simple hydrothermal method. The as-prepared nanostructured material displayed good purity and crystallinity, as well as high surface area. The MAF-5-Co^{II} NS

exhibited good redox activity, due to the occurrence of MAF-5-Co^{II}/MAF-5-Co^{III} redox pair. The redox system proved better catalytic activity toward the oxidation process of glucose, especially in alkaline medium. In addition, the sensor displayed high electrochemical stability and excellent repeatability and reproducibility in the different pH-based BP solutions with negligible interferences from common interfering compounds. It must be considered that, although the analytical performance of the MAF-5-Co^{II} NS/SPE sensor in PBS-diluted BP solution is lower compared to that in the NaOH-diluted BP solution, it is highly suitable for the direct detection of glucose by developing a disposable type sensor from the blood. Additionally, MAF-5-Co^{II} NS can be utilized as a potential catalytic electrode material to detect many other biologically important compounds due to its good stability in aqueous medium.

Supplementary Information The online version contains supplementary material available at https://doi.org/10.1007/s00604-021-04737-w.

Acknowledgements This work was financially supported by SPIN-Supporting Principal Investigators, Ca'Foscari University of Venice, Italy.

Compliance with ethical standards

Conflict of interest The authors declare that they have no competing interests.

References

1. Clark LC, Lyons C (1962) Electrode system for continuous monitoring in cardiovascular surgery. Ann N Y Acad Sci 102:29–45
2. Heller A, Feldman B (2008) Electrochemical glucose sensors and their applications in diabetes management. Chem Rev 108:2482–2505
3. Rahman MM, Ahammad AJS, Jin J-H, Ahn SJ, Lee JJ (2010) A comprehensive review of glucose biosensors based on nanostructured metal-oxides. Sensors 10:4855–4886
4. Hwang DW, Lee S, Seo M, Chung TD (2018) Recent advances in electrochemical non-enzymatic glucose sensors – a review. Anal Chim Acta 1033:1–34
5. Kim DM, Kim MY, Reddy SS, Cho J, Cho CH, Jung S, Shim YB (2013) Electron-transfer mediator for a NAD-glucose dehydrogenase-based glucose sensor. Anal Chem 85:11643–11649
6. Zhao M, Gao Y, Sun J, Gao F (2015) Mediatorless glucose biosensor and direct electron transfer type glucose/air biofuel cell enabled with carbon nanodots. Anal Chem 87:2615–2622
7. Wooten M, Karra S, Zhang M, Gorski W (2014) On the direct electron transfer, sensing, and enzyme activity in the glucose oxidase/carbon nanotubes system. Anal Chem 86:752–757
8. Zhu H, Li L, Zhou W, Shao Z, Chen X (2016) Advances in non-enzymatic glucose sensors based on metal oxides. J Mater Chem B 4:7333–7349
9. Tee SY, Teng CP, Ye E (2017) Metal nanostructures for non-enzymatic glucose sensing. Mater Sci Eng C 70:1018–1030
10. Si P, Huang Y, Wang T, Ma J (2013) Nanomaterials for electrochemical non-enzymatic glucose biosensors. RSC Adv 3:3487–3350
11. Wang R, Liang X, Liu H et al (2018) Non-enzymatic electrochemical glucose sensor based on monodispersed stone-like PtNi alloy nanoparticles. Microchim Acta 185:1–7
12. Ansari SA, Ahmed A, Ferdousi FK, Salam MA, Shaikh AA, Barai HR, Lopa NS, Rahman MM (2019) Conducting poly(aniline blue)-gold nanoparticles composite modified fluorine-doped tin oxide electrode for sensitive and non-enzymatic electrochemical detection of glucose. J Electroanal Chem 850:113394
13. Xu GR, Ge C, Liu D, Jin L, Li YC, Zhang TH, Rahman MM, Li XB, Kim W (2019) In-situ electrochemical deposition of dendritic Cu-Cu_2S nanocomposites onto glassy carbon electrode for sensitive and non-enzymatic detection of glucose. J Electroanal Chem 847:113177
14. Yan X, Gu Y, Li C, Zheng B, Li Y, Zhang T, Zhang Z, Yang M (2018) A non-enzymatic glucose sensor based on the CuS nanoflakes-reduced graphene oxide nanocomposite. Anal Methods 10:381–388
15. Liu Q, Zhong H, Chen M, Zhao C, Liu Y, Xi F, Luo T (2020) Functional nanostructure-loaded three-dimensional graphene foam as a non-enzymatic electrochemical sensor for reagentless glucose detection. RSC Adv 10:33739–33746
16. Lopa NS, Rahman MM, Ahmed F, Sutradhar SC, Ryu T, Kim W (2018) A Ni-based redox-active metal-organic framework for sensitive and non-enzymatic detection of glucose. J Electroanal Chem 822:43–49
17. Lopa NS, Rahman MM, Ahmed F, Ryu T, Lei J, Choi I, Kim DH, Lee YH, Kim W (2019) A chemically and electrochemically stable, redox-active and highly sensitive metal azolate framework for non-enzymatic electrochemical detection of glucose. J Electroanal Chem 840:263–271
18. Shahrokhian S, Ezzati M, Hosseini H (2020) Fabrication of a sensitive and fast response electrochemical glucose sensing platform based on co-based metal-organic frameworks obtained from rapid in situ conversion of electrodeposited cobalt hydroxide intermediates. Talanta 201:120696
19. Zhu X, Yuan S, Ju Y (2019) Water splitting-assisted electrocatalytic oxidation of glucose with a metal−organic framework for wearable nonenzymatic perspiration sensing. Anal Chem 91:10764–10771
20. Adeel M, Rahman MM, Caligiuri I, Canzonieri V, Rizzolio F, Daniele S (2020) Recent advances of electrochemical and optical enzyme-free glucose sensors operating at physiological conditions. Biosens Bioelectron 165:112331
21. Chinnadayyala SR, Park I, Cho S (2018) Nonenzymatic determination of glucose at near neutral pH values based on the use of Nafion and platinum black coated microneedle electrode array. Microchim Acta 185:250
22. Wang G, He X, Wang L, Gu A, Huang Y, Fang B, Geng B, Zhang X (2013) Non-enzymatic electrochemical sensing of glucose. Microchim Acta 180:161–186
23. Mei H, Sheng Q, Wu H, Zhang X, Wang S, Xia Q (2015) Nonenzymatic sensing of glucose at neutral pH values and low working potential using a glassy carbon electrode modified with platinum-iron alloy nanoparticles on a carbon support. Microchim Acta 182:2395–2401
24. Zhao L, Wu G, Cai Z, Zhao T, Yao Q, Chen X (2015) Ultrasensitive non-enzymatic glucose sensing at near-neutral pH values via anodic stripping voltammetry using a glassy carbon electrode modified with Pt3Pd nanoparticles and reduced graphene oxide. Microchim Acta 182:2055–2060
25. Muthuchamy N, Gopalan A, Lee KP (2018) Highly selective non-enzymatic electrochemical sensor based on a titanium dioxide

nanowire-poly(3-aminophenyl boronic acid)-gold nanoparticle ternary nanocomposite. RSC Adv 8:2138–2147
26. Branagan D, Breslin CB (2019) Electrochemical detection of glucose at physiological pH using gold nanoparticles deposited on carbon nanotubes. Sensors Actuators B Chem 282:490–499
27. Anik Ü, Timur S, Dursun Z (2019) Metal organic frameworks in electrochemical and optical sensing platforms: a review. Microchim Acta 186:1–15
28. Lopa NS, Rahman MM, Ahmed F, Chandra Sutradhar S, Ryu T, Kim W (2018) A base-stable metal-organic framework for sensitive and non-enzymatic electrochemical detection of hydrogen peroxide. Electrochim Acta 274:49–56
29. Hosseini H, Ahmar H, Dehghani A, Bagheri A, Tadjarodi A, Fakhari AR (2013) A novel electrochemical sensor based on metal-organic framework for electro-catalytic oxidation of L-cysteine. Biosens Bioelectron 42:426–429
30. Peng Z, Jiang Z, Huang X, Li Y (2016) A novel electrochemical sensor of tryptophan based on silver nanoparticles/metal-organic framework composite modified glassy carbon electrode. RSC Adv 6:13742–13748
31. Yuan B, Zhang R, Jiao X, Li J, Shi H, Zhang D (2014) Amperometric determination of reduced glutathione with a new co-based metal-organic coordination polymer modified electrode. Electrochem Commun 40:92–95
32. Sun Y, Li Y, Wang N, Xu QQ, Xu L, Lin M (2018) Copper-based metal-organic framework for non-enzymatic electrochemical detection of glucose. Electroanalysis 30:474–478
33. Bhadra BN, Seo PW, Khan NA, Jhung SH (2016) Hydrophobic cobalt-ethylimidazolate frameworks: phase-pure syntheses and possible application in cleaning of contaminated water. Inorg Chem 55: 11362–11371
34. Zhang JP, Zhang YB, Lin JB (2012) Metal azolate frameworks: from crystal engineering to functional materials. Chem Rev 112: 1001–1033
35. Zhu AX, Lin RB, Qi XL, Liu Y, Lin YY, Zhang JP, Chen XM (2012) Zeolitic metal azolate frameworks (MAFs) from ZnO/Zn(OH) 2 and monoalkyl-substituted imidazoles and 1,2,4-triazoles: efficient syntheses and properties. Microporous Mesoporous Mater 157:42–49
36. Wang M, Han J, Hu Y, Guo R (2017) Mesoporous C, N-codoped TiO_2 hybrid shells with enhanced visible light photocatalytic performance. RSC Adv 7:15513–15520
37. Li H, Gan S, Wang H, Han D, Niu L (2015) Intercorrelated superhybrid of AgBr supported on graphitic-C_3N_4 -decorated nitrogen-doped graphene: high engineering photocatalytic activities for water purification and CO_2 reduction. Adv Mater 27:6906–6913
38. Wen Y, Peng S, Wang Z, Hao J, Qin T, Lu S, Zhang J, He D, Fan X, Cao G (2017) Facile synthesis of ultrathin $NiCo_2S_4$ nano-petals inspired by blooming buds for high-performance supercapacitors. J Mater Chem A 5:7144–7152
39. Kwon HT, Jeong HK, Lee AS, An HS, Lee JS (2015) Heteroepitaxially grown zeolitic imidazolate framework membranes with unprecedented propylene/propane separation performances. J Am Chem Soc 137:12304–12311
40. Jiao Y, Pei J, Chen D, Yan C, Hu Y, Zhang Q, Chen G (2017) Mixed-metallic MOF based electrode materials for high performance hybrid supercapacitors. J Mater Chem A 5:1094–1102
41. Tomanin PP, Cherepanov PV, Besford QA, Christofferson AJ, Amodio A, McConville CF, Yarovsky I, Caruso F, Cavalieri F (2018) Cobalt phosphate nanostructures for non-enzymatic glucose sensing at physiological pH. ACS Appl Mater Interfaces 10:42786–42795
42. Nacef M, Chelaghmia ML, Affoune AM, Pontie M (2018) Electrochemical investigation of glucose on a highly sensitive nickel-copper modified pencil graphite electrode. Electroanalysis 31:113–120
43. Ko CY, Huang JH, Raina S, Kang WP (2013) A high performance non-enzymatic glucose sensor based on nickel hydroxide modified nitrogen-incorporated nanodiamonds. Analyst 138:3201–3208
44. Danaei G, Finucane MM, Lu Y, Singh GM, Cowan MJ, Paciorek CJ, Lin JK, Farzadfar F, Khang YH, Stevens GA, Rao M, Ali MK, Riley LM, Robinson CA, Ezzati M (2011) National, regional, and global trends in fasting plasma glucose and diabetes prevalence since 1980: systematic analysis of health examination surveys and epidemiological studies with 370 country-years and 2·7 million participants. Lancet 378:31–40